International Journal of Minerals, Metallurgy and Materials
Volume 22, Number 3, March 2015, Page 272
DOI: 10.1007/s12613-015-1071-5

Microstructural evolution of a heat-treated H23 tool steel

Meilinda Nurbanasari[1)], *Panos Tsakiropoulos*[2)], *and Eric J. Palmiere*[2)]

1) Department of Mechanical Engineering, Institut Teknologi Nasional, Bandung, Jl. PHH. Mustapha 23, Bandung, 40124, West Java, Indonesia

2) Department of Materials Science and Engineering, The University of Sheffield, Sir Robert Hadfield Building, Sheffield S1 3JD, United Kingdom

(Received: 22 May 2014; revised: 3 October 2014; accepted: 8 October 2014)

Abstract: The microstructure and the stability of carbides after heat treatments in an H23 tool steel were investigated. The heat treatments consisted of austenization at two different austenizing temperatures (1100°C and 1250°C), followed by water quenching and double-aging at 650°C, 750°C, and 800°C with air cooling between the first and second aging treatments. Martensite did not form in the as-quenched microstructures, which consisted of a ferrite matrix, M_6C, M_7C_3, and MC carbides. The double-aged microstructures consisted of a ferrite matrix and MC, M_6C, M_7C_3, and $M_{23}C_6$ carbides. Secondary hardening as a consequence of secondary precipitation of fine M_2C carbides did not occur. There was disagreement between the experimental microstructure and the results of thermodynamic calculations. The highest double-aged hardness of the H23 tool steel was 448 HV after austenization at 1250°C and double-aging at 650°C, which suggested that this tool steel should be used at temperatures below 650°C.

Keywords: tool steel; microstructural evolution; heat treatment; carbides; stability; hardness

1. Introduction

The high concentration of carbide-forming elements in tool steels encourages the formation of a carbide network in the as-cast microstructure, which can decrease the steels' toughness. The type of carbide, its volume fraction, morphology, size, and distribution can be modified through heat-treatment processes to achieve the required mechanical properties. H23 tool steel, which is one of the tungsten hot-work tool-steel groups, contains high concentrations of chromium and tungsten and is used for applications at elevated working temperatures (about 600°C) such as medium runs on brass die-casting dies. The H23 tool steel also has good hot strength and resistance to heat checking [1]. Previous studies [2–6] on the microstructure evolution and properties of hot-work tool steels after heat treatment showed a strong correlation between carbide precipitation and mechanical properties. Because the carbide affects the mechanical properties of the tool steel, the microstructure and types of carbide become very important. The carbide precipitation process during aging can be complicated when steels contain more than one carbide-forming element. Thomson and Bhadsehia [7] suggested that the sequence of carbide formation in high-chromium steels is matrix → M_3C → M_7C_3 → $M_{23}C_6$. Dudova and Kaibyshev [8] stated the carbide sequence in a 10% chromium steel is martensite → M_3C → M_2C → $M_{23}C_6$ and M_6C. Asadabad *et al.* [9] studied the aging of a 4.5%Cr–2%W–0.25%V (wt%) steel and observed that the M_3C and M_2C carbides formed in the first stages of aging and subsequently transformed into the M_7C_3 and $M_{23}C_6$ carbides.

Although numerous previous studies on tool steels have been reported [2–6], the microstructure changes, carbide precipitation, and mechanical properties of the heat-treated H23 tool steel have not been established. The difference in chemical composition and heat treatment of tool steel will also result in different microstructures and carbides that affect the mechanical properties of tool steels. Hence, in this study, we contribute to this growing area of research by exploring the microstructure and the stability of the carbide in H23 tool steel after heat treatment. We then compare the experimental results with those predicted using thermodynamic calculations.

Corresponding author: Meilinda Nurbanasari E-mail: meilinda@itenas.ac.id, nurbanasarimeilinda@yahoo.com

2. Experimental

A vacuum induction melting furnace was used to produce a square ingot of an H23 tool steel with nominal composition: 0.3%C–12.3%W–12.3%Cr–1.2%V–0.4%Mn–0.4%Ni–Fe balance (wt%) [10]. The 1-cm^3 samples for heat treatment were cut from the middle top of the ingots using an electric discharge machine. The samples were heated at 1100°C and 1250°C under an argon atmosphere with a 1-h holding time at each temperature and were subsequently water quenched. The water quenching was used to avoid grain coarsening and to achieve the optimum hardness. Double-aging was then conducted at three different aging temperatures of 650°C, 750°C, and 800°C, with a 1-h holding time at each temperature. Air cooling was performed between the first and second aging treatments. Groesbeck's etchant (100 mL of H_2O, 10 g of NaOH, and 10 g of $KMnO_4$) was used to reveal the carbides. The etching time was approximately 5–10 s. The optical microstructure observations were performed using an MET Polyvar microscope. The scanning electron microscopy (SEM) investigations were conducted on Inspect F (20 kV) and JEOL 6400 microscopes (20 kV), the latter of which was equipped with an energy-dispersive X-ray spectroscopy (EDS) unit; the INCA software was used for quantitative chemical analysis. All carbides larger than 0.1 μm as well as their volume fraction (V_c) based on SEM images were calculated using the ImageJ software. Thin foils for transmission electron microscopy (TEM) studies were prepared using electrolytic twin-jet polishing with a solution of 5vol% perchloric acid, 35vol% butoxyethanol, and 60vol% methanol. The TEM studies were conducted on a JEOL 2010F microscope (200 kV) equipped with an EDS unit operated using the Oxford ISIS software. A CV Instrument Vickers hardness tester was used to measure the hardness with a load of 10 kg. Phase and carbide identification were performed on a Siemens D5000 X-ray diffractometer equipped with a Co radiation source. The polished samples were scanned over the 2θ range of 30° to 130° at a 0.02° step size and a 1° per minute counting time. The STOE WinXPow software program and the ICDD (International Centre for Diffraction Data) files were used for peak identification. The calculated phase diagram of the H23 tool steel was obtained using the ThermoCalc software (TCEF6 database) [10].

3. Results and discussion

3.1. As-cast microstructure

Nurbanasari *et al.* [10] reported that the bulk hardness of cast H23 tool steel was 355 ± 4 HV and that the as-cast microstructure consisted of a ferrite matrix and carbides, as shown in Fig. 1. The carbides in the as-cast H23 tool steel were coarse tungsten-rich M_6C carbide, fine vanadium-rich MC carbide, and fine chromium-rich $M_{23}C_6$ carbide.

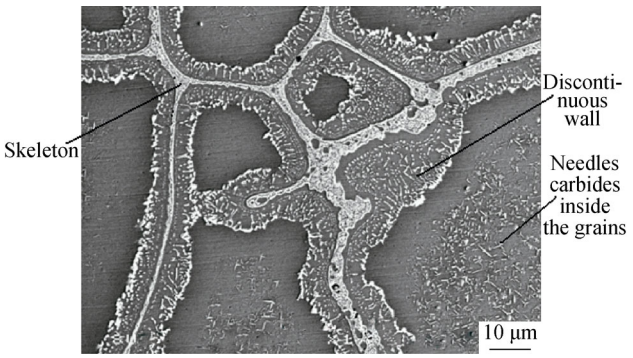

Fig. 1. Secondary-electron image of the as-cast H23 tool steel [10].

3.2. Effects of austenizing temperature

3.2.1. Effect of austenizing temperature on microstructure

Fig. 2 shows the as-quenched microstructures of the H23 tool steel prepared at two different austenizing temperatures. Ferrite and carbides coexisted, and no martensite was observed in the samples prepared at either austenizing temperatures because the Ms temperature of this tool steel is approximately −46°C [1]. Compared with the as-cast microstructure (Fig. 1), dissolution and separation of the carbides were observed in both austenized steels. In the sample austenized at the lower temperature, the carbides were still interconnected in the thick layer (skeleton) and carbides in the discontinuous wall dissolved. In the sample austenized at the higher temperature, the carbides in the skeleton became separated and coarser and the carbides in the discontinuous wall dissolved into the matrix to a greater extent. The microstructure of the as-quenched H23 tool steel austenized at the higher temperature exhibited a lower volume fraction of carbides because more carbide dissolved into the matrix. In the steel austenized at the higher temperature, a large volume fraction of undissolved M_6C carbides remained. The microstructures of the as-quenched H23 tool steel exhibited no indication of the inside-the-grain carbide needles observed in the as-cast steel (Fig. 1). These small needle carbides dissolved more easily into the matrix than the larger carbides because of their greater surface-to-volume ratio; i.e., smaller carbides were less stable than larger carbides of the same carbide type.

Figs. 3 and 4 show SEM images and EDS spectra of the matrix and carbides of the as-quenched H23 tool steel. Some

carbides exhibited two different contrasts under back scattered electron imaging conditions, which indicated that two types of coarse carbides formed in the as-quenched H23 tool steel. These carbides were identified by SEM–EDS as the M_6C (bright) and M_7C_3 carbides (grey), and this identification was supported by the XRD results (see Fig. 5), which confirmed the presence of α-Fe–Cr (the super-saturated solid solution), austenite, and the M_6C and M_7C_3 carbides. The M_6C carbide was Fe_3W_3C, and the M_7C_3 carbide was $(Cr,Fe)_7C_3$. Additional and more intense peaks associated with the Fe_3W_3C and $(Cr,Fe)_7C_3$ carbides were observed in the EDS spectra of the sample at austenized at 1100°C than in the spectrum of the sample austenized at 1250°C, which indicated that the volume fraction of these carbides was greater at the lower austenizing temperature. The following discussion shows that the dissolution rates of M_6C and M_7C_3 carbides differ and that a higher austenizing temperature results in the dissolution of more carbides into the matrix. No peaks associated with the $M_{23}C_6$ carbides were observed in the EDs spectra. Typical EDS spectra of the M_6C carbides (Figs. 3 and 4) showed intense tungsten and iron peaks. The typical EDS spectra of the M_7C_3 carbides exhibited an iron peak more intense than the chromium peak or vice versa [11–12]. Both types of carbides exhibited rod-like, irregular,

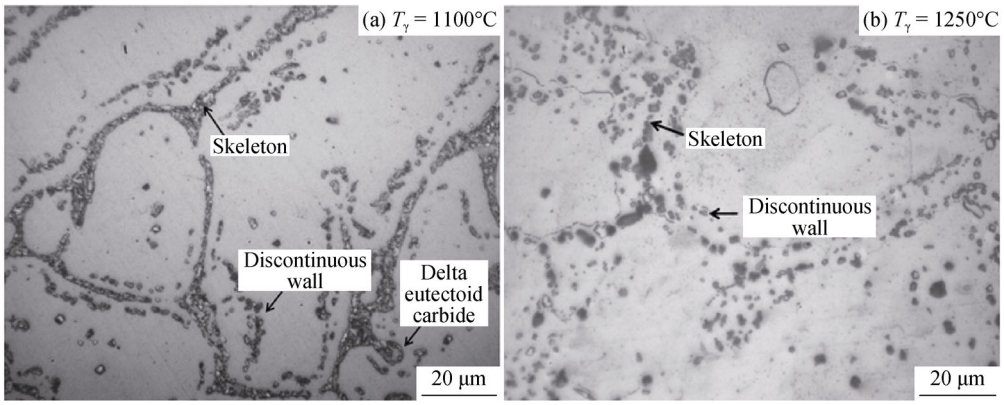

Fig. 2. Optical images of the microstructure of the H23 tool steel after austenization and water quenching.

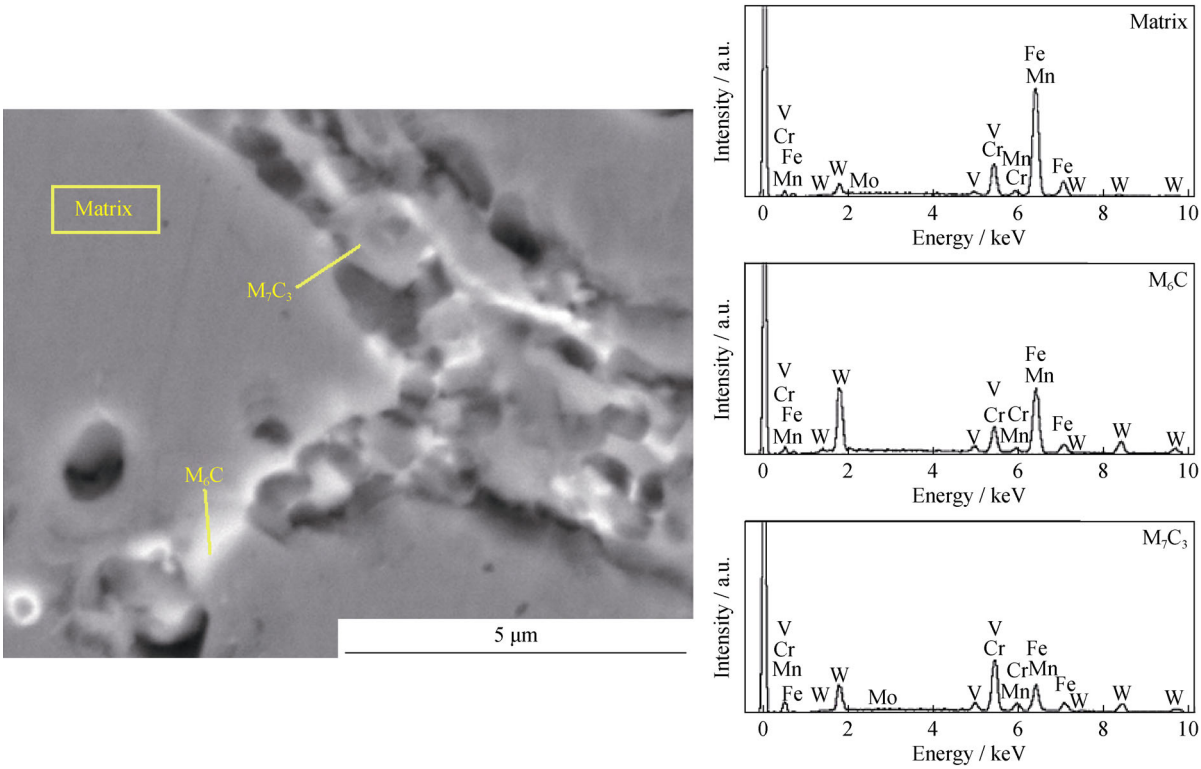

Fig. 3. Backscatter electron image of the H23 tool steel water quenched from T_γ = 1100°C and EDS spectra of the matrix and carbides.

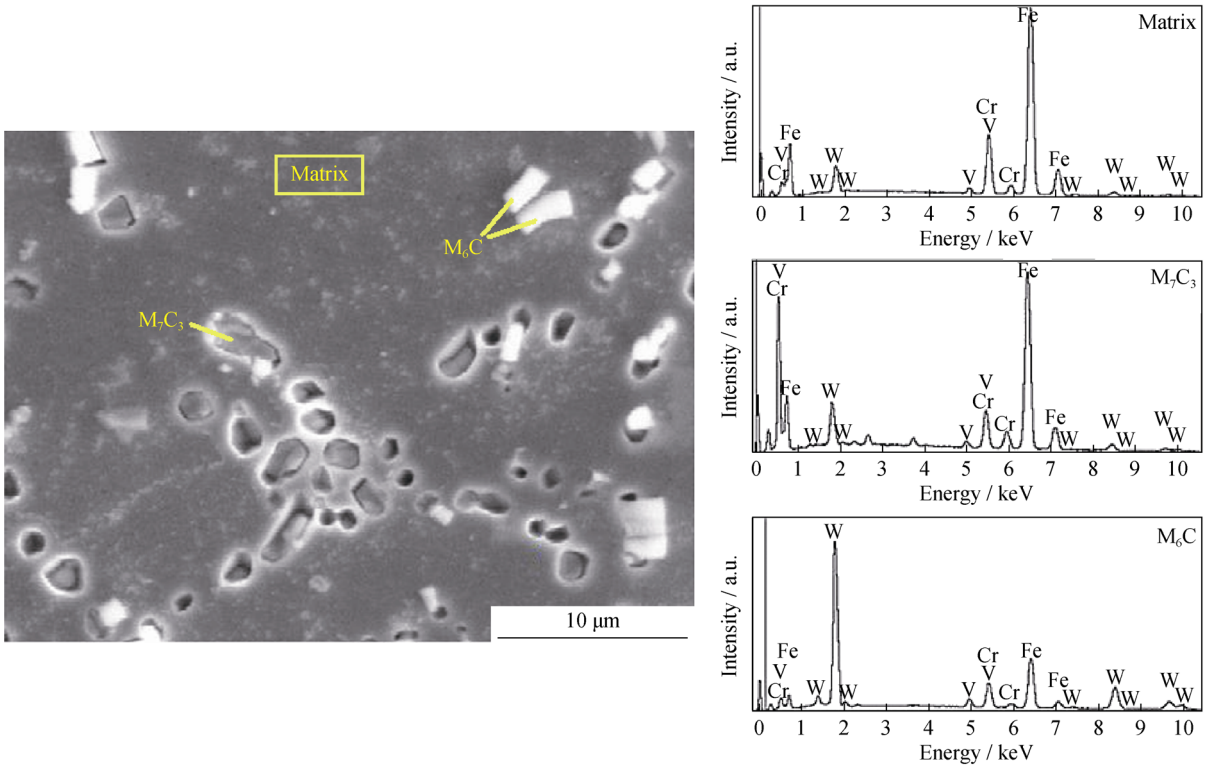

Fig. 4. Backscatter electron image of the H23 tool steel water quenched from T_γ = 1250°C and EDS spectra of the matrix and carbides.

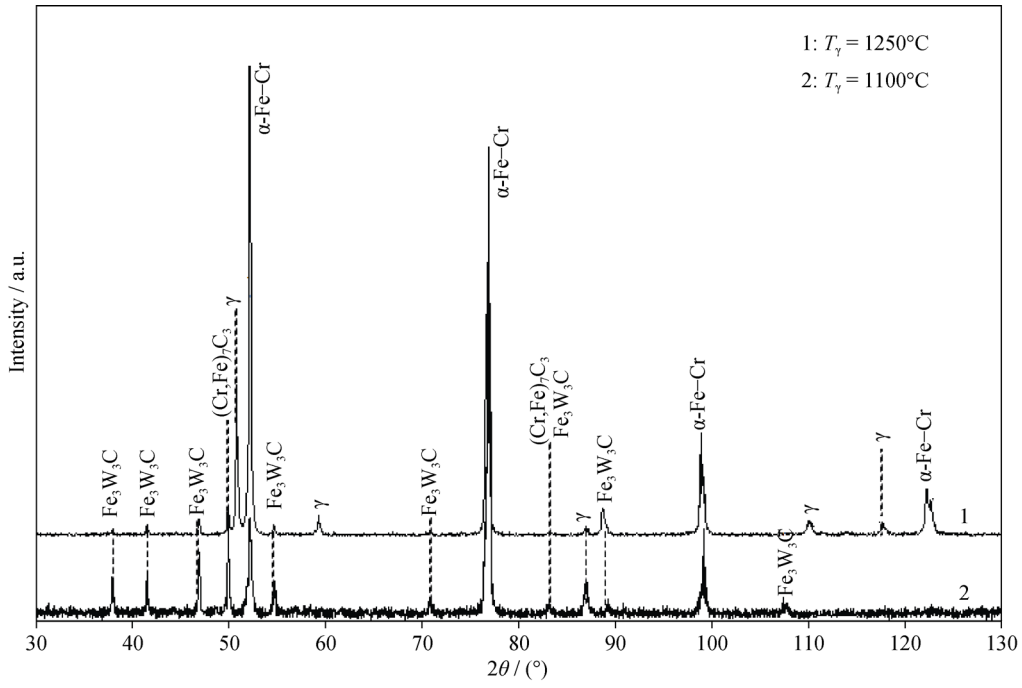

Fig. 5. X-ray diffraction pattern of the as-quenched H23 tool steel. The ICDD cards used were those of α-Fe–Cr (34–396), austenite (52–512), Fe_3W_3C (41–1351), and $(Cr,Fe)_7C_3$ (5–720).

and spherical morphologies. The presence of the $M_{23}C_6$ carbide in the as-quenched H23 tool steel austenized at both temperatures was not observed by either SEM or TEM. The $M_{23}C_6$ carbides easily coalesce and coarsen during austenization and could dissolve completely at about 1095°C [13–14]. Thus, the primary $M_{23}C_6$ carbides (i.e., the carbides

that formed upon solidification) dissolved gradually during austenization, thereby enriching the ferrite matrix with chromium and carbon and resulting in nucleation of the M_7C_3 carbide [15−16].

The quantitative data of the matrix and carbides measured using SEM–EDS are summarized in Table 1. The compositions of the matrices were in good agreement with those calculated using ThermoCalc-TCFE6 (79.9%Fe–13.1%Cr–1.1%V–5.9%W (wt%) at T_γ = 1100°C and 76.9%Fe–12.6%Cr–1.1%V–9.4%W (wt%) at T_γ = 1250°C). Table 1 also shows that the M_7C_3 carbide was rich in iron and chromium and that its chromium content decreased with increasing austenizing temperature. The diffusivity of alloying elements increases with increasing temperature and the diffusivity of chromium is higher than that of tungsten. Because the M_7C_3 carbide was rich in chromium, its dissolution was affected by its chromium content that reached its maximum value (and thus maximized the stability of the M_7C_3 carbide) at the austenizing temperature of 1100°C. The austenizing temperature at which the M_7C_3 carbide dissolves is higher than that at which the $M_{23}C_6$ carbide dissolves [17]. The dissolution rate of the M_7C_3 carbides was faster than that of the M_6C carbides, and the M_7C_3 carbides continued to dissolve at the higher austenizing temperature, where their chromium content decreased. This result contrasted that for the M_6C carbides, where the tungsten content increased with increasing austenizing temperature.

Table 1. SEM–EDS data of phases in the as-quenched H23 tool steel wt%

T_γ / °C	Phase	Element				Comment*
		Fe	Cr	V	W	
1100	Matrix	78.7 ± 0.6	13.8 ± 0.6	1.1 ± 0.0	6.5 ± 0.2	Ferrite
	Carbide	51.9 ± 5.7	13.0 ± 1.1	2.8 ± 0.2	32.4 ± 3.4	M_6C
	Carbide	50.0 ± 1.2	27.7 ± 0.3	3.3 ± 0.2	19.1 ± 0.3	M_7C_3
1250	Matrix	75.0 ± 0.9	14.0 ± 0.2	1.2 ± 0.0	9.8 ± 0.6	Ferrite
	Carbide	31.1 ± 6.6	9.1 ± 0.7	2.6 ± 0.2	56.9 ± 3.3	M_6C
	Carbide	76.1 ± 1.9	11.2 ± 1.2	1.1 ± 0.1	11.6 ± 0.9	M_7C_3

Note: * The quantitative data should be considered with caution given the size of the carbides.

Using SEM–EDS with accelerating voltage 20 kV requires a particle size greater than 1 μm for the analyzed carbide to obtain proper quantification without overlap from another constituent in the interaction volume. The quantitative data in Table 1 were taken from carbides with sizes in the range 0.3–1.5 μm. Thus, interference between the interaction volume of the matrix and the smaller carbides was unavoidable. In addition, on the basis of data in Table 1, a minor difference existed in the compositions of the alloying elements between the M_7C_3 carbides and the matrix at 1250°C because of the interference of the relatively large interaction volume with the matrix.

TEM studies were conducted on the sample austenized at the higher temperature to compliment the as-quenched microstructure characterization (see Fig. 6). The diffraction patterns of the austenite, ferrite, and MC carbide in Fig. 6 confirmed that these phases were present in the as-quenched microstructure. Because this tool steel contained high concentrations of ferrite-stabilizing elements (chromium and tungsten) and because its Ms temperature is far below room temperature [1], ferrite unsurprisingly existed in the as-quenched microstructure. The retained austenite observed in bright-field TEM images was a film type, with a width 10 to 60 nm and located at the ferrite lath boundaries. The formation of retained austenite was due to the dissolution of the carbides, which resulted in locally high carbon content in the matrix; water quenching from the higher austenizing temperature did not provide sufficient time for the austenite to completely transform to ferrite. The size of the MC carbides was about 40 to 50 nm. The MC carbide and the ferrite matrix exhibited the Baker–Nutting relationship [18].

3.2.2. Effect of austenizing temperature on hardness

The hardness of the as-quenched tool steel was 279 ± 1 HV and 302 ± 7 HV after being quenched from austenizing temperatures of 1100°C and 1250°C, respectively. The as-quenched hardness of the tool steel was lower than the hardness of the cast steel because the austenite did not transform to martensite. The higher hardness of the as-quenched tool steel austenized at the higher temperature was attributed to the dissolution of carbides into the matrix, which enriched the matrix with alloying elements. The high tungsten and chromium contents in the H23 tool steel stabilized the presence of delta ferrite at the austenizing temperature. This ferrite was stable to room temperature and

did not contribute to hardening. Thus, the lower hardness with decreasing austenizing temperature was not only due to the lower dissolution of carbides, but was also due to the higher volume fraction of ferrite and the non-transformation of austenite to martensite because of the low Ms temperature.

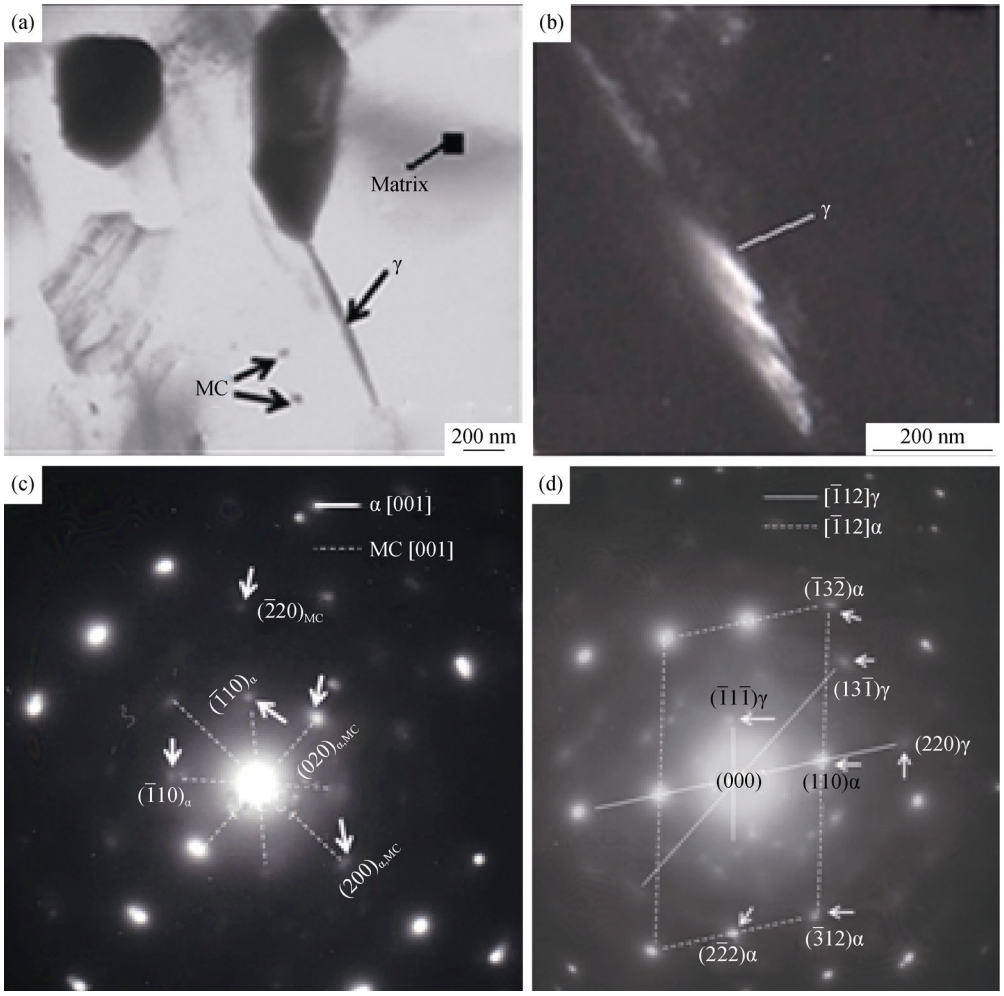

Fig. 6. Top row: bright-field TEM image showing MC carbides, ferrite (matrix), and retained austenite in the H23 tool steel austenized at 1250°C and water quenched (a) and dark-field TEM image showing retained austenite (b). Bottom row: selected-area diffraction patterns (SADPs) of the MC carbide in the ferrite matrix (c) and the retained austenite and ferrite (d).

Table 2 shows that the austenizing temperature strongly influenced the volume fraction of carbides, which decreased with increasing austenizing temperature, and subsequently enriched the matrix with alloying elements via the dissolution of carbides, whose extent of dissolution increased in the sequence MC, M_6C, M_7C_3, $M_{23}C_6$ [19]. The correlation between the mean size of carbides and the austenizing temperature was not conclusive because the mean size of carbides was measured for individual carbides and the carbide networks still existed at the lower austenizing temperature.

Table 2. Volume fraction of carbides and their average size in the H23 tool steel water quenched from different austenizing temperatures

As cast condition		As quenched condition			
		T_γ = 1250°C		T_γ = 1100°C	
V_c / %	Mean size / μm	V_c / %	Mean size / μm	V_c / %	Mean size / μm
21.5 ± 0.4	0.4 ± 0.1	13.9 ± 1.0	0.5 ± 0.1	15.3 ± 1.9	0.4 ± 0.2

3.3. Effect of double-aging treatment

3.3.1. Effect of double-aging treatment on microstructure

The microstructure evolution of tool steels is distinctly affected by the different aging conditions. Fig. 7 shows the microstructure of the H23 tool steel after treatment at different austenizing and double-aging temperatures. The double-aged microstructures austenized at different tempera-

tures consisted of ferrite and carbides. In general, the carbides were more separated in their prior network after austenization at the higher temperature and were still interconnected in their prior network after austenization at the lower temperature; in addition, the undissolved delta ferrite was also observed in the sample austenized at the lower temperature. Fig. 7 also shows that, in the samples austenized at the higher temperature, fine secondary carbides were observed after the double-aging treatment at 650°C; in contrast, in the sample austenized at the lower temperature, fine secondary carbides were observed under double-ageing at 750°C. The volume fraction of secondary carbides was higher in the samples austenized at the higher temperature than in the samples austenized at the lower temperature when the same double-aging temperature was used. This greater volume fraction was due to the increased dissolution of carbides at the higher austenizing temperature causing more carbon to be dissolved in the matrix, which provided the driving force for carbide precipitation during the double-aging process [6].

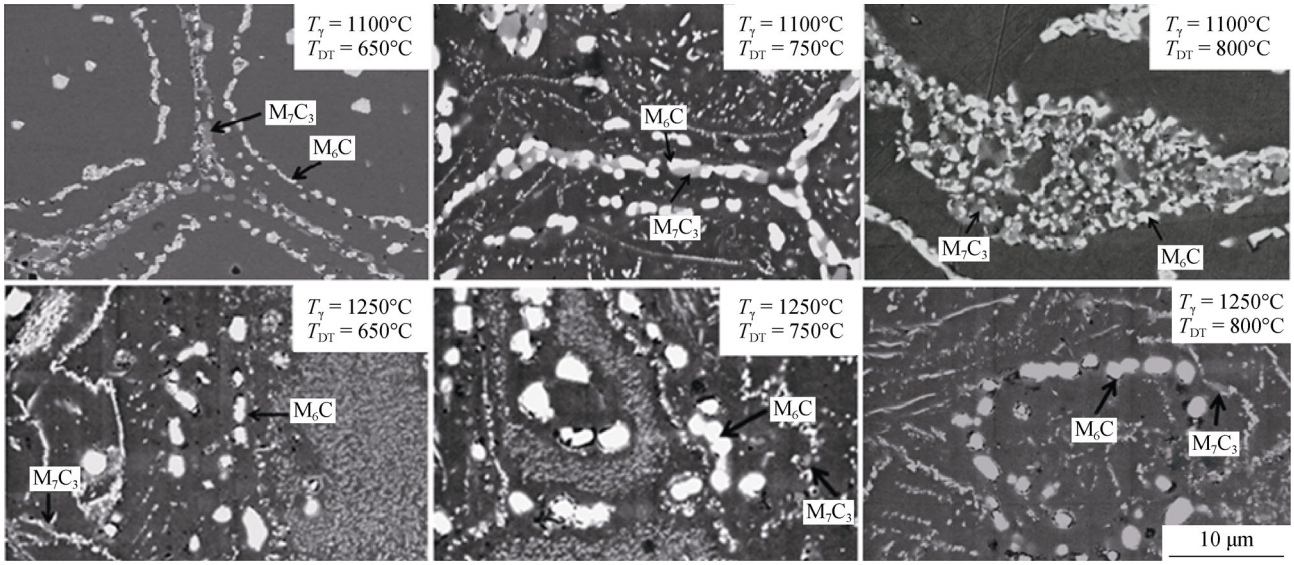

Fig. 7. Backscatter electron images of the H23 tool steel austenized and double-aged at various temperatures.

The presence of retained austenite after water quenching also affected the secondary carbide precipitation process during aging. The retained austenite phase continually transformed during the first and second aging procedures. The decomposition of the retained austenite was accompanied by further precipitation of carbides [20], which reduced austenite stability, resulting in transformation from austenite to ferrite during the cooling process. Fig. 7 also shows that, with increasing aging temperature, the fine carbides coalesced; as a result, the fine carbides tended to disappear when the samples were aged at 800°C. Because this process is controlled by diffusion, an increase in the aging temperature allowed sufficient time for the carbides to grow.

The dominant carbide in all of the double-aged samples was the M_6C carbide, followed by the M_7C_3 carbide. The volume fraction of the $M_{23}C_6$ carbides was smaller than that of the M_7C_3 carbides. The different contrast of carbides in the SEM backscatter electron images was used to differentiate the type of carbide. In Fig. 8, the precipitates exhibited three different contrasts. The carbides with greater atomic number than that of the matrix exhibited white contrast (M_6C); carbides that exhibited grey ($M_{23}C_6$) and lighter-grey (M_7C_3) contrast were also observed. The main metallic elements in the carbides were chromium, iron, vanadium, and tungsten. The SEM–EDS data for the dominant carbides M_6C and M_7C_3 are given in Table 3. Notably, when the M_7C_3 and $M_{23}C_6$ carbides were analyzed at a spatial resolution of about 1 μm, interference occurred not only with the matrix but also with other carbide types. Because the volume fraction of the $M_{23}C_6$ carbides was small, only a few quantitative analyses were possible. The intensities of the chromium and iron peaks in the spectra of the $M_{23}C_6$ carbides were similar (the iron/chromium count ratio was about 1). The quantitative EDS data for the $M_{23}C_6$ carbides showed that their average composition was 3.2%V–40.9%Cr–40.4%Fe–15.5%W (wt%). The EDS data showed that the M_6C carbides were rich in tungsten, the M_7C_3 carbides were rich in chromium and tungsten, and the $M_{23}C_6$ and M_7C_3 carbides were rich in chromium, with the chromium and tungsten contents in the $M_{23}C_6$ carbides being respectively higher and lower than those in the M_7C_3 carbide. Thus, the M_7C_3 carbides exhibited a lighter grey contrast

than the $M_{23}C_6$ carbides. Notably, the M_6C and M_7C_3 carbides were formed in the as-quenched microstructures; therefore, the M_6C and M_7C_3 carbides in the double-aged sample were undissolved primary carbides and secondary carbides. The primary $M_{23}C_6$ carbides dissolved during austenization and formed as secondary $M_{23}C_6$ carbides during double-aging. The M_7C_3 carbides were observed in two different sites; they coexisted with others carbide types, which indicated that they had formed via *in situ* transformation, and they were not joined with other carbide types, which indicated that they had formed individually in the matrix [21]. The M_6C carbides were present in all of the samples, and the $M_{23}C_6$ carbides coexisted with the M_7C_3 and M_6C carbides. These three carbide types had spherical and irregular morphologies.

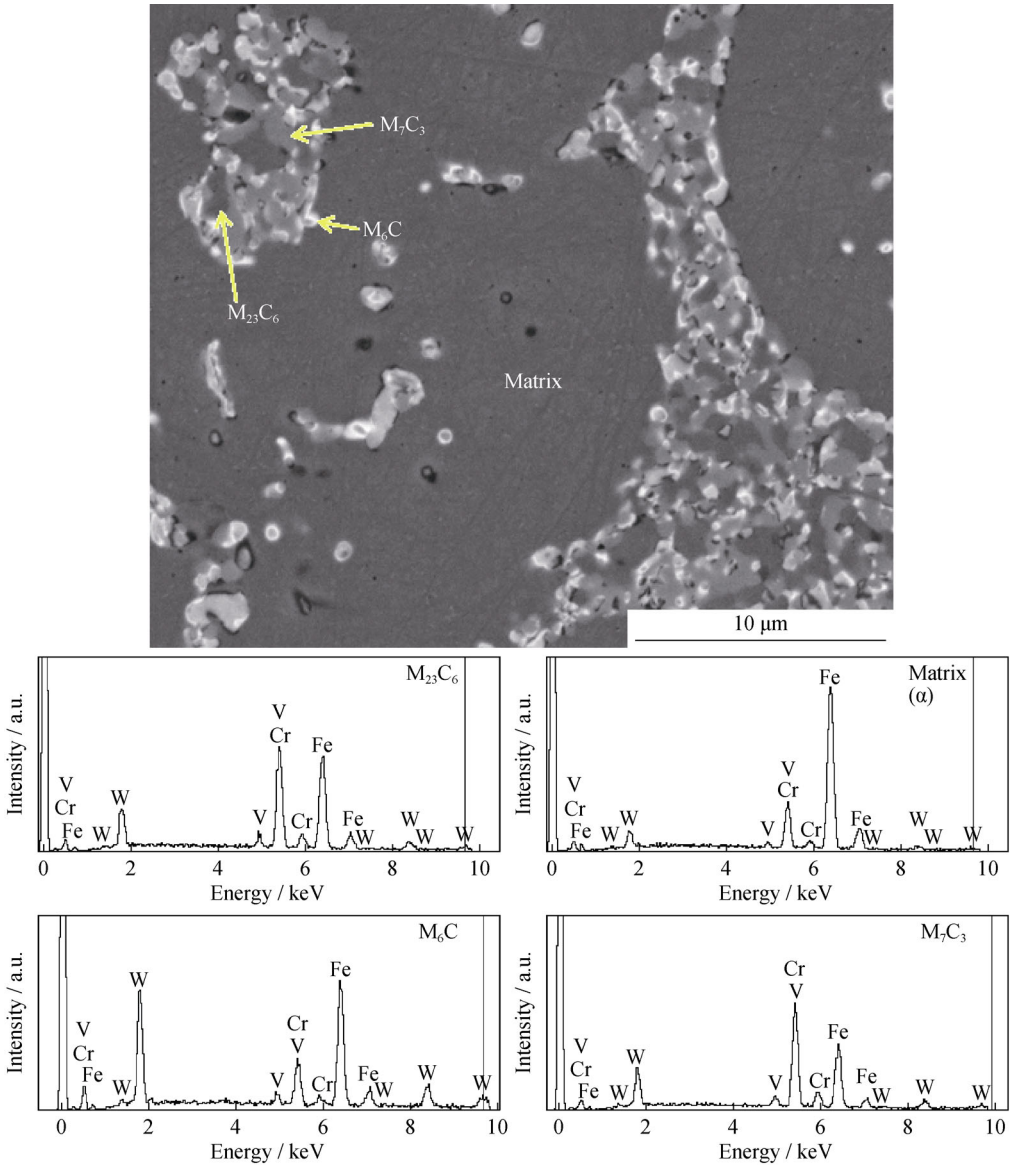

Fig. 8. Backscatter electron image and EDS spectra of the matrix and carbides in the H23 tool steel austenized at 1100°C and double-aged at 650°C.

Data in Table 3 would suggest that, at an austenizing temperature of 1100°C, the chromium content in the M_7C_3 carbide increased at aging temperatures up to 750°C and then decreased significantly after aging at 800°C, whereas the tungsten content in the M_7C_3 carbides increased with increasing aging temperature. In the sample aged at 650°C, the M_7C_3 carbides were very fine (Fig. 7), and as the aging temperature was increased to 750°C, these carbides grew and their composition moved closer to the equilibrium value. As the aging temperature was increased further to 800°C, the M_7C_3 carbides began to lose their stability and their chromium contents decreased. Notably, the M_7C_3 carbide is

rich in chromium and the diffusivity of chromium is greater than those of tungsten and vanadium. Thus, after austenization at 1100°C, the M_7C_3 carbides became unstable when aged at temperatures greater than 750°C. The chromium content in the M_7C_3 carbides was lower at an austenizing temperature of 1250°C than at an austenizing temperature of 1100°C when the same aging temperature was used, which indicated that the M_7C_3 carbides in the sample austenized at the higher temperature were not stable at an aging temperature of 650°C. This finding is consistent with the results of a previous study [6] in which the authors reported that a higher austenizing temperature accelerated the carbides' approach to equilibrium. The evolution of the chemical composition of the M_6C carbides was different than that of the M_7C_3 carbides. The tungsten content of the M_6C carbides was higher at the austenizing temperature of 1250°C than at 1100°C when the aging temperature was the same. This higher tungsten content is attributed to the matrix becoming richer in tungsten at the higher austenizing temperature because more carbides had dissolved in it. The tungsten content in the M_6C carbides in the double-tempered sample also increased with increasing aging temperature. When precipitated at 650°C, the secondary M_6C carbides were fine and their composition was far from the equilibrium value. With increasing aging temperature, the carbides grew by consuming more tungsten to approach the equilibrium composition. However, their tungsten content did not decrease after the steel was aged at 800°C, which indicated that these carbides still grew and did not reach equilibrium. Because the growth of carbides is controlled by diffusion (time and temperature dependence) and the diffusivity of tungsten is lower than that of the other alloying elements, more time and/or a higher temperature is required for the M_6C carbides to become unstable. Fig. 9 shows a bright-field TEM image of MC, M_6C, and M_7C_3 carbides formed in the H23 tool steel double-tempered at 750°C; the TEM image does not show Fe_3C or M_2C carbides. These latter carbides might have formed in the early stages of transformation and dissolved quickly with increasing aging temperature. Baker and Nutting [22] also studied the precipitation sequence of carbides in ferritic microstructures in a 2.25%Cr–1%Mo (wt%) steel. The ferrite contained M_2C carbides. Subsequent aging led to the dissolution of the M_2C and its replacement by the more stable M_6C carbides. In the present work, the M_7C_3 carbides nucleated between pre-existing M_6C carbides or the M_6C carbides acted as nucleation sites for M_7C_3 secondary carbides. Fine MC carbides were observed in the matrix; however, no evidence of the $M_{23}C_6$ carbides was observed.

Table 3. SEM–EDS results of carbides in the double-aged H23 tool steel wt%

T_γ / °C	T_{DA} / °C	Element				Comment*
		Fe	Cr	V	W	
1100	650	54.6 + 3.1	11.8 ± 0.3	0.9 ± 0.1	32.7 ± 3.2	M_6C
	750	48.7 ± 3.3	11.9 ± 2.6	2.6 ± 0.1	36.5 ± 2.0	
	800	39.5 ± 5.2	11.8 ± 1.6	1.9 ± 0.1	46.9 ± 2.6	
	650	44.8 ± 3.6	35.2 ± 4.0	3.1 ± 0.1	16.9 ± 0.4	M_7C_3
	750	34.5 ± 0.1	38.8 ± 0.1	3.7 ± 0.1	23.0± 0.2	
	800	60.7 ± 6.4	13.2 ± 1.1	1.3 ± 0.6	24.8 ± 4.7	
1250	650	37.1 + 5.3	11.8 ± 1.2	2.4 ± 0.2	48.7 ± 5.9	M_6C
	750	28.1 ± 2.2	8.3 ± 0.1	2.6 ± 0.2	61.0 ± 2.1	
	800	25.6 ± 2.4	8.7 ± 0.4	2.5 ± 0.2	63.1 ± 2.8	
	650	46.4 ± 1.8	19.6 ± 0.8	2.2 ± 0.1	31.7 ± 1.0	M_7C_3
	750	70.5 ± 2.5	16.3 ± 2.6	1.4 ± 0.2	11.9 ± 0.5	
	800	77.2 ± 2.1	12.3 ± 1.3	1.0 ± 0.1	9.5 ± 0.3	

Note: * The quantitative data should be considered with caution given the size of carbides; T_{DA} is the double-aging temperature.

3.3.2. Carbide evolution

Four types of carbides were observed in the double-aged H23 tool steel: MC, M_6C, M_7C_3, and $M_{23}C_6$ carbides. The dominant carbides formed under the double-aging conditions were the M_6C and M_7C_3 carbides. The formation of the M_6C carbide at the expense of the $M_{23}C_6$ carbide was not observed. Secondary M_6C carbides formed within the tungsten-rich matrix via dissolution of the M_2C carbides. Al-

though the Fe_3C carbides were not observed in all of the double-aged microstructures, we hypothesized that this type of carbide precipitated below the aging temperature of 650°C and transformed quickly into the chromium-rich carbides M_7C_3 and $M_{23}C_6$. The $M_{23}C_6$ carbides grew with increasing aging temperature and gradually disappeared from the microstructure after the sample was aged at 800°C. The M_7C_3 carbide either formed via the reaction $M_3C \rightarrow M_7C_3 + M_{23}C_6$ or nucleated directly from ferrite (separate or individual nucleation). In the former case, the reaction started by the increase of the chromium content in the M_3C carbide and the M_7C_3 carbide particles grew. The M_7C_3 carbide was more dominant than the $M_{23}C_6$ carbide in the double-aged H23 tool steel because of the presence of vanadium in the steel, which tends to stabilize the M_7C_3 carbide phase [23]. Bjärbo and Hättestrand [24] have reported that a competition occurs between the nucleation and growth processes of the M_7C_3 and $M_{23}C_6$ carbides, and in high-chromium-content tool steel, the $M_{23}C_6$ carbide would nucleate at the same time as the M_7C_3 carbide. We concluded that the Fe_3C transformed into M_7C_3 carbide, and a small volume fraction of M_3C likely transformed into $M_{23}C_6$ carbide. Therefore, the carbide evolution in the H23 tool steel occurred as follows. *in situ* transformation: Matrix $\rightarrow M_3C \rightarrow M_7C_3 + M_{23}C_6$; separate transformation: Matrix $\rightarrow M_3C \rightarrow M_2C \rightarrow M_6C$ and Matrix $\rightarrow M_7C_3$.

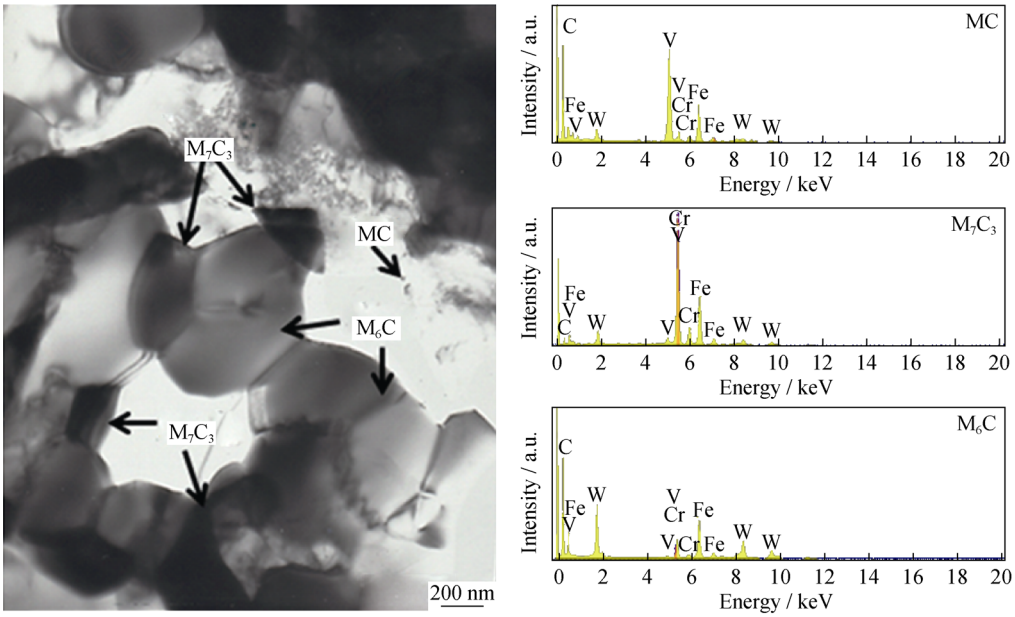

Fig. 9. Bright-field TEM image of the H23 tool steel water quenched from 1100°C and double-aged at 750°C and EDS spectra of carbides.

The XRD diffractograms in Fig. 10 confirmed the presence of solid-solution ferrite (α-Fe–Cr), the M_6C, $M_{23}C_6$, and M_7C_3 carbides. The MC carbide was not identified by XRD; however, its presence was confirmed by TEM [10]. The low volume fraction of the MC carbide and the overlap of its peaks with those of the M_7C_3 and $M_{23}C_6$ carbides [25] precluded its detection by XRD. Fig. 10 also shows that the XRD peaks of the M_6C carbide were dominant and the intensity of the XRD peaks of the M_7C_3 carbide was higher than that of the $M_{23}C_6$ carbide under all double-aging conditions. The XRD results were in good agreement with the other microstructure studies regarding the high volume fraction of the M_6C carbides and the dominance of the M_7C_3 over the $M_{23}C_6$ carbides.

3.3.3. Effect of double-aging treatment on hardness

The precipitation of carbides during aging significantly contributed to the final hardness of the tool steel. The effects of the austenizing and double-aging temperatures on the hardness of the H23 tool steel are shown in Fig. 11. Fig. 11 shows that the hardness of the double aged H23 tool steel increased with increasing austenizing temperature and decreased with increasing double-aging temperature. The highest hardness (448 HV) was achieved in the case of the sample austenized at 1250°C and double aged at 650°C. This result is attributable to the carbides dissolving more extensively into the matrix with increasing austenizing temperature, thereby providing a high nucleation rate of carbide precipitation during the double-aging process [6]. Double-

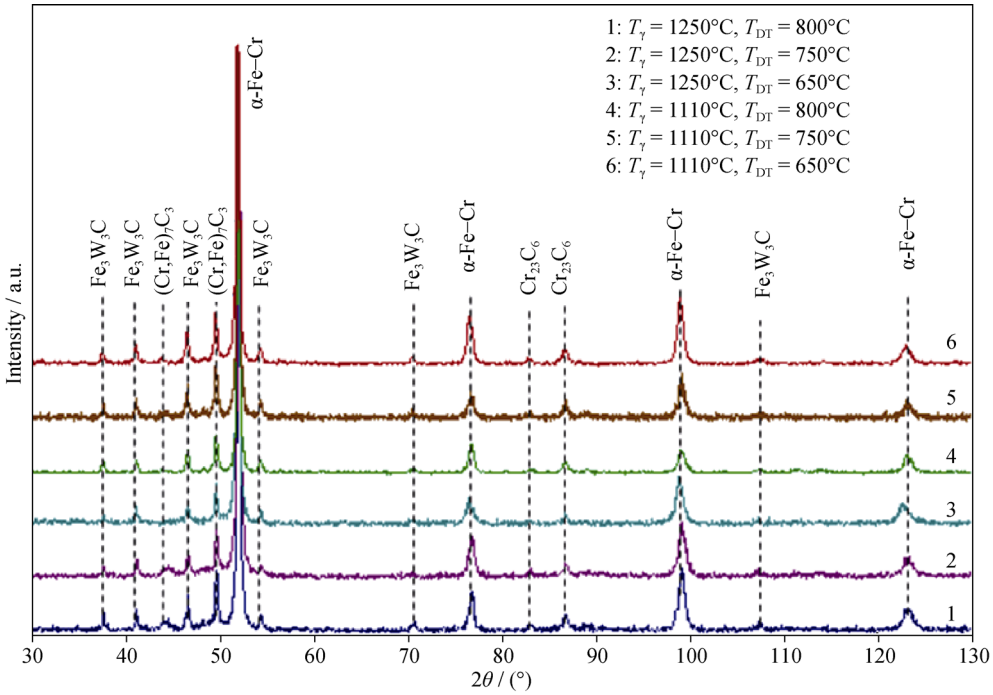

Fig. 10. XRD diffraction pattern of the H23 tool steel with different austenization and double-aging temperatures. The ICDD cards used were α-Fe–Cr (34–396), austenite (52–512), Fe_3W_3C (41–1351), $Cr_{23}C_6$ (35–783), and $(Cr,Fe)_7C_3$ (5–720).

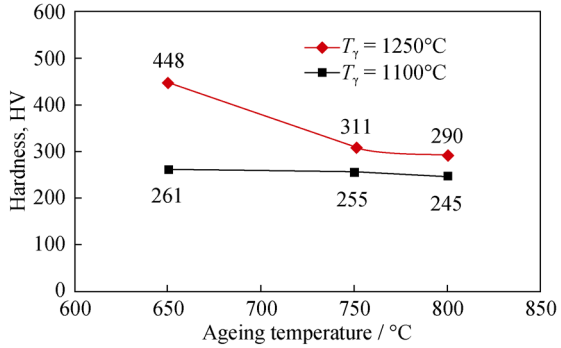

Fig. 11. Effect of austenization and double-aging temperatures on the hardness of the H23 tool steel.

aging at temperatures of 650°C and 800°C did not reveal a secondary hardening peak, which has been correlated to fine M_2C carbides [1]. In the microstructure of the double-aged H23 tool steel, unstable M_2C or M_3C carbides were not observed. The higher chromium content in the H23 tool steel caused these unstable carbides to dissolve at temperatures below 650°C. Quantitative data of carbide size and volume fraction for the three double-aging temperatures are given in Table 4.

Table 4 shows that the volume fraction of carbides slightly increased with increasing aging temperature, which was attributed to the precipitation of secondary carbides; more of these carbides precipitated at the higher aging temperature because of the greater diffusivity of the alloying elements. The secondary carbides formed during the double-aging process of the H23 tool steel were M_6C and chromium-rich carbides M_7C_3 and $M_{23}C_6$. The latter carbides reached their equilibrium composition and dissolved at lower temperature compared to the M_6C carbide; in addition, increasing austenizing temperature accelerated the approach of the chromium-rich carbides to equilibrium during aging at 650°C. Hence, no significant difference in the volume fraction of carbides was observed between steels aged at 750°C and 800°C. In addition, no correlation was observed between the average size of carbides and aging temperature, likely because coalesced carbides formed networks that

Table 4. Volume fraction and average size of carbides in the H23 tool steel austenized and double-aged at various temperatures

T_γ / °C	Double ageing temperature / °C					
	650		750		800	
	V_c / %	Mean size / μm	V_c / %	Mean size / μm	V_c / %	Mean size / μm
1100	16.0 ± 0.2	0.3 ± 0.1	17.7 ± 0.5	0.2 ± 0.2	18.2 ± 0.3	0.3 ± 0.2
1250	16.9 ± 0.3	0.3 ± 0.1	18.3 ± 0.6	0.3 ± 0.1	18.5 ± 0.4	0.3 ± 0.2

made the measurements of carbide size less accurate. The average carbide size in the double-aged H23 tool steel increased with increasing aging temperature when the steel was austenized at 1250°C because of a reduction in the total area of the ferrite/carbide interphase boundary. The overall impression from the microstructure studies was that carbides were slightly coarsened with increasing aging temperature. We concluded that the decrease of hardness with increasing aging temperature was due to the carbides coarsening and ferrite grain growth. This conclusion suggests that the peak of secondary hardening of the H23 tool steel occurred at temperatures below 650°C.

3.4. Equilibrium microstructure at 600°C

The calculated isopleth phase diagram is shown in Fig. 12, where the vertical dotted line indicates the composition of the steel used in this study. According to the phase diagram, the equilibrium microstructure of this steel at 600°C should consist of ferrite, $M_{23}C_6$ carbide, and a Fe_2W Laves phase. To verify the thermodynamic calculations, the H23 tool steel was austenized at 1250°C for 1 h, water quenched, and then heat treated at 600°C for 400 h. According to the XRD data shown in Fig. 13, the phases present in the microstructure were ferrite and the M_6C and $M_{23}C_6$ carbides. No peaks corresponding to the Fe_2W Laves phase were observed, which we attributed either to the absence of this phase in the microstructure of the steel or its presence at a volume fraction below the detection limit of the X-ray diffractometer. Given the XRD results, the experimental microstructure and the results of the thermodynamic calculation did not agree with each other.

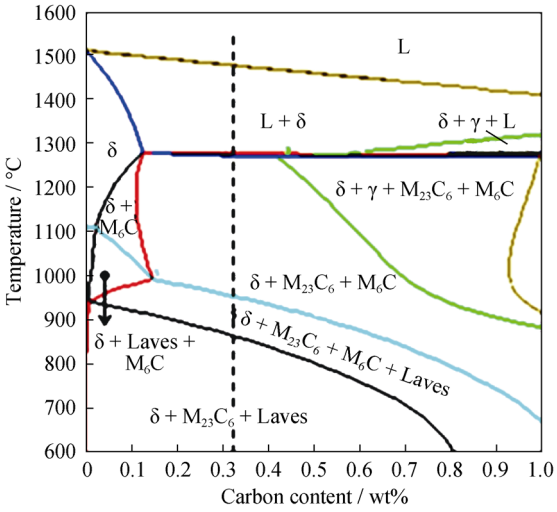

Fig. 12. Calculated isopleth of the H23 tool steel phase diagram [10].

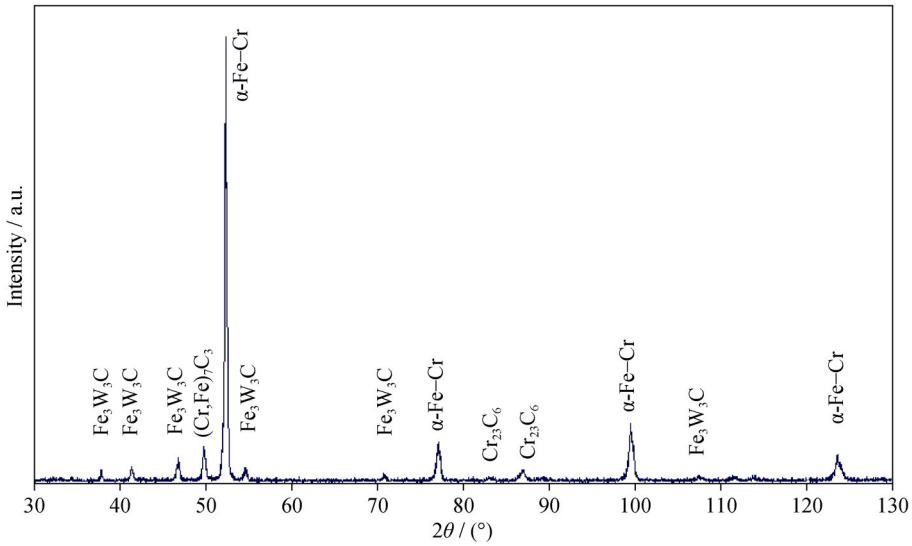

Fig. 13. XRD diffraction pattern of the H23 tool steel water quenched from T_γ = 1250°C and single aging at 600°C for 400 h. The ICDD cards used were those of α-Fe–Cr (34–396), austenite (52–512), Fe_3W_3C (41–1351), $Cr_{23}C_6$ (35–783), and $(Cr,Fe)_7C_3$ (5–720).

4. Conclusions

In this paper, the effect of austenization and double-aging treatments on the microstructure and hardness of H23 tool steel were studied. The following conclusions were drawn:

(1) The M_6C (Fe_3W_3C), M_7C_3 ($(Cr,Fe)_7C_3$), and MC carbides were formed in the as-quenched steels austenized at 1100°C and 1250°C.

(2) The chromium content of the M_7C_3 carbides tended to decrease at higher austenizing and aging temperatures, and the tungsten content of the M_6C carbides increased with increasing austenizing and aging temperatures.

(3) The MC, M_6C, M_7C_3, and $M_{23}C_6$ carbides were observed in the microstructure after the double-aging treatment,

and M_6C and M_7C_3 were the dominant carbides.

(4) The secondary M_6C carbides formed during double-aging because of the dissolution of M_2C carbides.

(5) The approach of carbides to their equilibrium composition during double-aging was strongly affected by the austenizing temperature.

(6) The maximum hardness of the double-aged H23 tool steel (448 HV) was achieved via austenization at 1250°C followed by double-aging at 650°C.

Acknowledgements

The author (MN) would like to express great appreciation to the Directorate of Higher Education, Indonesian Government and to the Institut Teknologi Nasional (Itenas), Bandung, Indonesia for their financial support.

References

[1] G.A. Roberts, G. Kraus, and R.L. Kennedy, *Tool Steels*, Materials Park, ASM International, Ohio, 1998.

[2] M.L. Fares, M. Athmani, Y. Khelfaoui, and A. Khettache, An investigation into the effects of conventional heat treatments on mechanical characteristics of new hot working tool steel, *IOP Conf. Ser. Mater. Sci. Eng.*, 28(2012), No. 1, art. No. 012024.

[3] P. Bała and J. Krawczyk, Transformation during quenching and ageing of hot-work tool steel, *Hradec Moravici*, 19(2009), p. 1.

[4] Z. Zhang, D. Delagnes, and G. Bernhart, Microstructure evolution of hot-work tool steels during tempering and definition of a kinetic law based on hardness measurements, *Mater. Sci. Eng. A*, 380(2004), p. 222.

[5] A. Medvedeva, J. Bergström, S. Gunnarsson, and J. Andersson, High temperature properties and microstructural stability of hot work tool steels, *Mater. Sci. Eng. A*, 523(2009), No. 1-2, p. 39.

[6] M. Nurbanasari, P. Tsakiropoulos, and E.J. Palmiere, A study of carbide precipitation in a H21 tool steel, *ISIJ Int.*, 54(2014), No. 7, p. 1667.

[7] R.C. Thomson and H.K.D.H. Bhadeshia, Carbide precipitation in 12Cr1MoV power plant steel, *Metall. Trans. A*, 23(1992), p. 1171.

[8] N. Dudova and R. Kaibyshev, On the precipitation sequence in a 10% Cr steel under tempering, *ISIJ Int.*, 51(2011), No. 5, p. 826.

[9] M.A. Asadabad, S. Kheirandish, and A.J. Novinrooz, Tempering behavior of 4.5Cr–2W–0.25V steel, *J. Iron Steel Res. Int.*, 17(2010), No. 10, p. 57.

[10] M. Nurbanasari, P. Tsakiropoulos, and E.J. Palmiere, On the solidification of a H23 tool steel, *Trans. Indian Inst. Met.*, 67(2014), No. 6, p. 935.

[11] N. Mebarki, D. Delagnes, P. Lamesle, F. Delmas, and C. Levaillant, Relationship between microstructure and mechanical properties of a 5% Cr tempered martensitic tool steel, *Mater. Sci. Eng. A*, 387-389(2004), p. 171.

[12] A.M. Elrakayby and B. Mills, Identification of carbides in high-speed steels, *J. Mater. Sci. Lett.*, 5(1986), p. 332.

[13] F. Abe, H. Araki, and T. Noda, The effect of tungsten on dislocation recovery and precipitation behavior of low-activation martensitic 9Cr steels, *Metall. Trans. A*, 22(1991), p. 2225.

[14] F.B. Pickering, The properties of tool steels for mould and die applications [in] G. Krauss and H. Nordberg, eds., *Tool Materials for Molds and Dies*: *Application and Performance*, CSM Press Golden, Colorado, 1987, p. 3.

[15] D.J. Dyson and K.W. Andrews, Carbide M_7C_3 and its formation in alloy steels, *J. Iron Steel Inst.*, 207(1969), No.2, p.208.

[16] K. Kuo, Carbides in chromium, molybdenum, and tungsten steels, *J. Iron Steel Inst.*, 173(1953), p. 363.

[17] R. Wilson, *Metallurgy and Heat Treatment of Tool Steel*, Mc Graw-Hill, London, 1975.

[18] G.E. Totten, L. Xie, and K. Funatani, *Handbook of Mechanical Alloy Design*, Marcel Dekker Inc, New York, 2004.

[19] S. Karagoz and H. Fischmeister, Microstructure and toughness in high speed tool steels: the influence of hot reduction and austenitization temperature, *Steel Res.*, 58(1987), No. 8, p. 353.

[20] A. Saha Podder and H.K.D.H. Bhadeshia, Thermal stability of austenite retained in bainitic steels, *Mater. Sci. Eng. A*, 527(2010), No. 7-8, p. 2121.

[21] G.J. Cai, H.O. Andren, and L.E. Svensson, Microstructural change of a 5% Cr steel weld metal during tempering, *Mater. Sci. Eng. A*, 242(1998), No. 1-2, p. 202.

[22] R.G. Baker and J. Nutting, The tempering of 2.25Cr%–1%Mo steel after quenching and normalizing, *J. Iron Steel Inst.*, 202 (1959), p. 257.

[23] H.K.D.H. Bhadeshia and R.W.K. Honeycombe, *Steels*: *Microstructure and Properties*, Elsevier Ltd., Oxford, 2006.

[24] A. Bjärbo and M. Hättestrand, Complex carbide growth, dissolution and coarsening in a modified 12 pct chromium steel-an experimental and theoretical study, *Metall. Mater. Trans. A*, 32 (2001), No. 1, p. 19.

[25] K. Asakura, A. Kohyama, and T. Yamada, Mechanical properties and microstructure changes of low-activation 3Cr–2W–V–Ti ferritic steels developed for nuclear applications, *ISIJ Int.*, 30(1990), No. 11, p. 947.